Generation of High-Quality Single-Photon Sources in Cavity Optomagnonics

Rui Hou(侯瑞)[1], Wei Zhang(张微)[2], Xue Han(韩雪)[1*], Hong-Fu Wang(王洪福)[1*], and Shou Zhang(张寿)[1*]

[1]*Department of Physics, College of Science, Yanbian University, Yanji 133002, China*
[2]*School of Physics, Harbin Institute of Technology, Harbin 150001, China*

(Received 9 November 2024; accepted manuscript online 24 December 2024)

We propose a scheme for generating high-quality single-photon sources utilizing the conventional photon blockade (CPB) effect in a cavity optomagnonic system with Kerr nonlinearity. The realization of the CPB effect depends on both the Kerr nonlinearity and Kerr-like nonlinearity of the optical cavity, which is converted using magneto-optical coupling. The CPB effect can be realized in a cavity optomagnonic system with weak magneto-optical coupling by modulating the strength of the Kerr nonlinearity. Notably, our scheme supports photon blockade in both the strong and weak Kerr nonlinear regimes, which broadens the range of experimental parameters. Furthermore, we explored the parameter regimes where the CPB effect could not be achieved because of the combined effects of the magneto-optical coupling and Kerr nonlinearity. We also determined the optimal driving amplitude region for generating high-quality single-photon sources. This work not only provides a novel route for realizing the CPB effect but also establishes a versatile platform for producing single-photon sources with high purity and brightness.

DOI: 10.1088/0256-307X/42/1/014203 CSTR: 32039.14.0256-307X.42.1.014203

1. Introduction. Hybrid quantum systems based on collective spin excitations (i.e., magnons) in ferromagnetic crystals have become crucial platforms for novel quantum technologies,[1–6] offering multitasking capabilities beyond individual components by combining various quantum subsystems. Yttrium iron garnet (YIG) is a ferromagnetic material with high spin density ($\rho \sim 4.22 \times 10^{27}\,\mathrm{m}^{-3}$), which is widely used to realize a strong coupling effect between microwave photons and the magnons inside the material.[7–9] Various quantum phenomena based on microwave photon–magnon coupling, such as magnon–photon–phonon entanglement,[10,11] mechanical squeezing,[12–14] and magnon blockade,[15,16] have been extensively investigated both theoretically and experimentally. The coupling between magnons and photons in the optical regime differs from that in the microwave regime. In the microwave regime, the frequency matching condition supports linear microwave photon–magnon coupling. Conversely, the photon–magnon coupling in the optical regime is parametric due to a frequency mismatch. This parametric optomagnonic coupling relies on the Faraday effect,[17] in which the angle of polarization of the light changes as it propagates through a magnetic material.

Cavity optomagnonics,[18–22] which describes the optomagnonic coupling between optical whispering gallery modes (WGMs) and magnon modes in a YIG sphere, has recently garnered widespread attention and contributed to significant progress in the field of quantum information. Examples of this progress include coherent optical-to-microwave conversion,[23,24] magnon induced transparency,[25] Brillouin light scattering,[26–28] periodic photon–magnon blockade,[29] and chaos.[30–32] On the other hand, conventional photon blockade (CPB), which originates from the anharmonicity of a system's eigenenergy spectrum, has been demonstrated in various systems, including cavity quantum electrodynamics,[33–35] quantum dot cavity,[36,37] cavity optomechanical,[38–40] and cavity optomagnonic systems.[41] It is widely acknowledged that strong magnon–photon coupling has been achieved in the microwave regime. However, the strength of optomagnonic coupling in the optical regime is significantly weaker than the typical decay rates of magnons and photons[26] (on the order of MHz and GHz, respectively). Thus, an intriguing question arises: How can the CPB effect be achieved in a cavity optomagnonic system characterized by weak optomagnonic coupling?

In this Letter, we propose an experimentally feasible scheme to achieve the CPB effect in a cavity optomagnonic system without requiring strong optomagnonic coupling. We determined the condition for single-photon resonance transition by analyzing the eigenvalues of the Hamiltonian. The numerical results were in good agreement with the analytical calculations, which confirmed the validity of our analysis. When this condition was satisfied, the CPB effect exhibited a strong dependence on both the optomagnonic coupling and Kerr nonlinearity. We also investigated the impact of the strength of the photon Kerr nonlinearity on the statistical properties of photons in both strong and weak nonlinear regimes. Specifically, we found that Kerr nonlinearity was essential for achieving photon antibunching. The results in this study may provide guidance for achieving robust CPB effect in hybrid optomagnonic sys-

*Corresponding author. Email: xuehan@ybu.edu.cn; hfwang@ybu.edu.cn; szhang@ybu.edu.cn
© 2025 Chinese Physical Society and IOP Publishing Ltd. All rights, including for text and data mining, AI training, and similar technologies, are reserved.

tems.

This letter is organized as follows. Section 2 introduces the physical model. Subsequently, we solve analytically for the eigenvalue of the reduced Hamiltonian. In Section 3, we analytically and numerically solve the equal-time second-order correlation functions. Section 4 discusses the effect of tunable parameters on the CPB. Finally, a conclusion is given in Section 5.

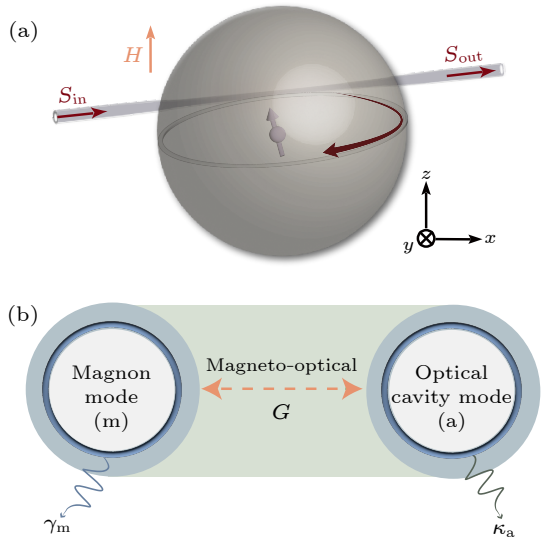

Fig. 1. Schematic configuration of the model considered. (a) An optomagnonic cavity with homogeneous magnetization along the z axis and a localized optical mode, a, with circular polarization in the x-y plane. Here, $S_{\rm in}$ and $S_{\rm out}$ denote the input and output fields, respectively. (b) The homogeneous magnon mode couples to the optical mode with strength G. $\kappa_{\rm a} = \omega_{\rm a}/Q$ and $\gamma_{\rm m}$ represent the decay rates of the optical and magnon modes, respectively.

2. System Model. In our scheme, the optomagnonic cavity is a single-crystal YIG sphere with a radius of 400 μm. Owing to the symmetry of the sphere, light is confined within the sphere by the total internal reflection, resulting in WGMs. As a result, the YIG sphere simultaneously supports both optical WGMs and magnon modes, with the coupling mechanism based on the Faraday effect. The input light, which is characterized by amplitude ε and frequency $\omega_{\rm d}$, couples evanescently to the optical WGM via a tapered fiber, as shown in Fig. 1(a). The Hamiltonian of the hybrid cavity optomagnonic system is as follows (setting $\hbar = 1$):

$$H_0 = \omega_{\rm a} a^\dagger a - \Omega \hat{S}_z + G\hat{S}_x a^\dagger a + U a^\dagger a^\dagger a a + \varepsilon(a^\dagger e^{-i\omega_{\rm d} t} + a e^{i\omega_{\rm d} t}). \tag{1}$$

Here, a ($a^\dagger$) represents the annihilation (creation) operator of the optical cavity mode with frequency $\omega_{\rm a}$. Considering a magnetically ordered system characterized by dimensionless macrospin $\hat{\boldsymbol{S}} = (\hat{S}_x, \hat{S}_y, \hat{S}_z)$, with magnetization axis along $\hat{z}$, precession frequency $\Omega = \gamma_0 H$ is adjustable via external bias magnetic field H. The parametric optomagnonic coupling induced by the Faraday magneto-optical effect is realized through the interaction dynamics between circularly polarized optical WGMs and the x-component of the collective spin operator. Figure 1(b) illustrates that the optical field couples only to the x-component of macrospin $\hat{\boldsymbol{S}}$, with coupling coefficient G depending on the material. $U = 3(\hbar\omega_{\rm a})^2\chi^{(3)}/(4\varepsilon_0\varepsilon_r^2 V_{\rm eff})$ is the Kerr nonlinear strength of the optical cavity mode. Given a large spin density, we can employ the Holstein–Primakoff transformation to map spin operators onto the creation and annihilation operators of bosons, with the transformations given by

$$\begin{aligned} \hat{S}_x &= \sqrt{S/2}(m + m^\dagger), \\ \hat{S}_z &= S - m^\dagger m. \end{aligned} \tag{2}$$

Here, $S = |\hat{\boldsymbol{S}}|$, and $\hat{S}_x$ and $\hat{S}_z$ represent the x- and z-components of the spin operator, respectively. This transformation serves as the starting point for our subsequent discussion, allowing us to replace spin operator $\hat{\boldsymbol{S}}$ with magnon m. Therefore, the Hamiltonian of the system can be written as follows:

$$\begin{aligned} H' &= \omega_{\rm a} a^\dagger a + \Omega m^\dagger m + G\sqrt{S/2} a^\dagger a (m + m^\dagger) \\ &\quad + U a^\dagger a^\dagger a a + \varepsilon(a^\dagger e^{-i\omega_{\rm d} t} + a e^{i\omega_{\rm d} t}). \end{aligned} \tag{3}$$

To eliminate the time-dependent terms, in the rotating frame defined by $V = \exp(-i\omega_{\rm d} a^\dagger a t)$, the transformed Hamiltonian, $H_1 = V^\dagger H' V + i\dot{V}^\dagger V$, can be written as follows:

$$\begin{aligned} H_1 &= \Delta_{\rm a} a^\dagger a + \Omega m^\dagger m + G\sqrt{S/2} a^\dagger a (m + m^\dagger) \\ &\quad + U a^\dagger a^\dagger a a + \varepsilon(a^\dagger + a), \end{aligned} \tag{4}$$

where $\Delta_{\rm a} = \omega_{\rm a} - \omega_{\rm d}$ is the driving detuning. In order to clearly observe the impact of nonlinear optomagnonic coupling on the anharmonicity of the system's eigenenergy, we further implement a unitary transformation, $V_1 = \exp[g a^\dagger a(m^\dagger - m)/\Omega]$ (with $g = G\sqrt{S/2}$). Through this transformation, the nonlinear optomagnonic coupling term is effectively diagonalized and thus transformed into a Kerr-like nonlinearity of the optical cavity. Given that the coupling strength is usually small (i.e., $g \ll \Omega$), the transformed Hamiltonian, $H_2 = V_1^\dagger H_1 V_1$, can be approximated as follows:

$$\begin{aligned} H_2 &= (\Delta_{\rm a} - U) a^\dagger a + \Omega m^\dagger m + \left(U - \frac{g^2}{\Omega}\right)(a^\dagger a)^2 \\ &\quad + \varepsilon(a^\dagger + a). \end{aligned} \tag{5}$$

Based on the Hamiltonian in Eq. (5), it is evident that the magnon part decouples from the system. When focusing solely on the optical characteristics of the system, the magnon part can be neglected. Therefore, the reduced Hamiltonian is given by

$$H_3 = (\Delta_{\rm a} - U) a^\dagger a + \left(U - \frac{g^2}{\Omega}\right)(a^\dagger a)^2 + \varepsilon(a^\dagger + a). \tag{6}$$

This reduced Hamiltonian can be viewed as a Kerr nonlinear cavity system, where the Kerr coefficient is determined by Kerr nonlinear strength U, nonlinear optomagnonic coupling strength g, and magnon frequency Ω. The underlying physical mechanism of the CPB effect is the anharmonicity of the eigenenergy spectrum of the system. Although the magnon part is not explicitly included in the reduced Hamiltonian, it still influences the CPB effect of the system. To analyze the CPB effect in the system, it

is necessary to understand the eigenvalues of Hamiltonian H_3. Under weak driving condition (i.e., setting $\varepsilon = 0$), the eigenvalue equation for the Hamiltonian H_3 can be written as follows:

$$H_3|n\rangle = E_n|n\rangle. \tag{7}$$

We can determine the corresponding eigenvalue as follows:

$$E_n = (\Delta_\mathrm{a} - U)n + (U - g^2/\Omega)n^2, \tag{8}$$

where $|n\rangle$ represents the eigenstate, and n denotes the photon number. Clearly, both the Kerr nonlinearity and optomagnonic coupling contribute to the shift in the photon energy levels. Furthermore, the energy difference, $\Delta E = E_{n+1} - E_n$, is not a constant value, which leads to a detuning of the transition between the single-excited and two-excited states when a resonance transition is formed between the zero-excited and single-excited states. Consequently, this detuning results in the generation of a single-photon blockade (PB) effect.

3. Statistical Properties of Photons. In the field of quantum optics, the performance of a single-photon source is typically characterized by two key parameters: the purity and brightness. The former is described by the equal-time second-order correlation function,

$$g_\mathrm{a}^{(2)}(0) = \frac{\langle a^\dagger a^\dagger a a\rangle}{\langle a^\dagger a\rangle^2}, \tag{9}$$

and the latter is defined as the average photon numbers,

$$N_\mathrm{a} = \langle a^\dagger a\rangle. \tag{10}$$

To investigate the statistical properties of photons in a hybrid cavity optomagnonic system, we obtain analytical and numerical results for the photon correlation functions by solving the non-Hermitian Schrödinger equation and quantum master equation, respectively.

3.1. Analytical Solution. We derive an approximate analytical expression for the statistical properties of photons by solving the Schrödinger equation: $i\partial|\psi(t)\rangle/\partial t = H_\mathrm{non}|\psi(t)\rangle$, where $H_\mathrm{non} = H_3 - i\kappa_\mathrm{a} a^\dagger a/2$. Under the weak driving condition ($\varepsilon \ll \kappa_\mathrm{a}, \gamma_\mathrm{m}$), the evolution space can be restricted to the two excitation subspaces. Consequently, the wave function of the system is $|\psi(t)\rangle = C_0(t)|0\rangle + C_1(t)|1\rangle + C_2(t)|2\rangle$, where $C_n(t)$ denotes the probability amplitude of the state, $|n\rangle$. These probability amplitudes satisfy the relation $|C_0| \simeq 1 \gg |C_1| \gg |C_2|$. When $t \to \infty$, using the perturbation method, we approximately obtain the analytical solution of $g_\mathrm{a}^{(2)}(0)$ as follows:

$$g_\mathrm{a}^{(2)}(0) = \frac{\langle a^\dagger a^\dagger a a\rangle}{\langle a^\dagger a\rangle^2} \simeq \frac{2|C_2|^2}{|C_1|^4}. \tag{11}$$

3.2. Numerical Simulation. In addition to analytically solving the photon correlation functions, the dynamical evolution of the system can also be achieved through numerical simulations of the quantum master equation. The numerical simulation process not only verifies the accuracy of the above analytical calculations, but also provides the flexibility to manipulate the evolutionary space of the system to test whether higher numbers of photon excitations are completely suppressed. The dynamical evolution of the system is governed by the quantum master equation:

$$\dot{\rho} = -i[H_1, \rho] + \frac{\kappa_\mathrm{a}}{2}\mathcal{L}[a]\rho + \frac{\gamma_\mathrm{m}}{2}\mathcal{L}[m]\rho, \tag{12}$$

where $\mathcal{L}[o]\rho = 2o\rho o^\dagger - o^\dagger o\rho - \rho o^\dagger o$ is the Lindblad term and ρ is the density operator of the system. It can be observed that the calculations of the master equation are based on Hamiltonian H_1. Compared to the analytical calculations, the numerical simulation of the master equation is exact, involving no approximations. Therefore, a comparison of the numerical and analytical solutions further validates the effectiveness of all the approximate calculations. When the system reaches a steady state, the equal-time second-order photon correlation function of the output field is expressed as follows:

$$g_\mathrm{a}^{(2)}(0) = \frac{\langle a_\mathrm{out}^{\dagger 2} a_\mathrm{out}^2\rangle}{\langle a_\mathrm{out}^\dagger a_\mathrm{out}\rangle^2} = \frac{\mathrm{Tr}(a^\dagger a^\dagger a a \rho_s)}{[\mathrm{Tr}(a^\dagger a \rho_s)]^2}. \tag{13}$$

Different values of $g_\mathrm{a}^{(2)}(0)$ correspond to different effects and statistical properties, as listed in Table 1.

Table 1. Different values of the second-order correlation function.

Value	Statistics	Effect
$g_\mathrm{a}^{(2)}(0) > 1$	Super-Poissonian	Bunching (tunneling)
$g_\mathrm{a}^{(2)}(0) < 1$	Sub-Poissonian	Antibunching (blockade)

4. Results. We initially focus on the CPB effect in the strong nonlinear regime (i.e., $U > \kappa$). Figure 2 illustrates $\ln[g_\mathrm{a}^{(2)}(0)]$ and N_a as functions of the detuning $\Delta_\mathrm{a}/\kappa_\mathrm{a}$ for different values of Kerr nonlinear strength U. The points and curves in the figure correspond to the exact numerical solutions and analytical results, respectively, and their consistency confirms the validity of Eq. (11) and its associated approximations. Meanwhile, we observe that the photon antibunching effect is gradually enhanced with an increase in Kerr nonlinear strength U. The dips in $g_\mathrm{a}^{(2)}(0)$ indicate a sub-Poissonian behavior, which is a characteristic of the PB effect. In contrast, the peaks in $g_\mathrm{a}^{(2)}(0)$ exhibit a super-Poissonian behavior, which indicates that photon tunneling leads to multi-photon transitions. At the same time, we find that the average photon number at the detuning corresponding to the peak of $g_\mathrm{a}^{(2)}(0)$ is greater than zero, which confirms the presence of super-Poisson statistics. Remarkably, we observe that the maximum average photon number corresponds precisely with the location of the strongest PB effect. This finding reveals that our system is capable of generating high-quality single-photon sources with high purity and brightness when the single-photon resonance transition condition is satisfied.

Moreover, we also studied the PB effect in the weak nonlinear regime (i.e., $U < \kappa$), and the results are presented in Fig. 3(a). The results show that the photon antibunching effect gradually decreases with U. Notably, although the minimum value of $g_\mathrm{a}^{(2)}(0)$ is larger than that in the strong nonlinear regime, the PB effect can still be observed. Figure 3(b) further depicts $\ln[g_\mathrm{a}^{(2)}(0)]$ as a function of Kerr nonlinear strength U under the single-photon resonance transition condition (i.e., $\Delta_\mathrm{a} = g^2/\Omega$). The results clearly show that $g_\mathrm{a}^{(2)}(0)$ gradually decreases as U

increases. This indicates that our system can achieve the PB effect in both the strong and weak nonlinear regimes, thereby expanding the range of experimental parameter conditions. Particularly, in the absence of Kerr nonlinearity (i.e., $U = 0$), $g_{\rm a}^{(2)}(0) \to 1$, which indicates that the system is unable to create the PB effect. Therefore, Kerr nonlinearity stands as a necessary condition for achieving the PB effect in our system. Because both Kerr nonlinear strength U and optomagnonic coupling strength g contribute to the eigenvalue of the system, we further investigate the effect of g on the CPB effect. In Fig. 3(c), we plot $\ln[g_{\rm a}^{(2)}(0)]$ as a function of $g/\kappa_{\rm a}$ for different values of U. We observe that the value of $\ln[g_{\rm a}^{(2)}(0)]$ gradually increases with g. This phenomenon can be attributed to the increase in g, leading to a decrease in $(U - g^2/\Omega)$, which weakens the CPB effect. Therefore, it is necessary to maintain a weak optomagnonic coupling strength. Meanwhile, under the condition of a constant optomagnonic coupling strength, g/κ, we observe a significant enhancement of the PB effect with an increase in Kerr nonlinear strength U.

In order to visualize the PB effect more clearly, we plot function $\ln[g_{\rm a}^{(2)}(0)]$ versus optomagnonic coupling strength g/κ and Kerr nonlinear strength U/κ in Fig. 3(d). The white dotted line corresponds to the values of U that satisfy the following condition: $U = g^2/\Omega$. It is observed that when $U = g^2/\Omega$, the system cannot achieve the PB effect. This conclusion is supported by the theoretical analysis provided by Eq. (6), which indicates that at $U = g^2/\Omega$, the energy levels exhibit a harmonic behavior. Figure 3(d) further demonstrates that both g and U have significant effects on the PB. Given the weak optomagnonic coupling ($g = 2\pi \times 6\,\text{Hz}$), a larger Kerr nonlinearity is required to achieve a strong PB effect.

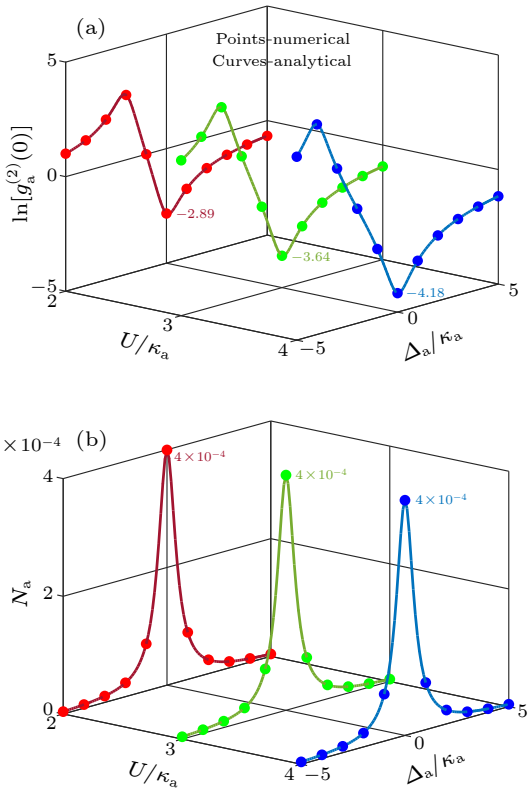

Fig. 2. (a) $\ln[g_{\rm a}^{(2)}(0)]$ versus $\Delta_{\rm a}/\kappa_{\rm a}$ for different values of U. (b) $N_{\rm a}$ versus $\Delta_{\rm a}/\kappa_{\rm a}$ for different values of U. Kerr nonlinear strength U is set to 2, 3, and 4 $\kappa_{\rm a}$. The analytical results utilize Hamiltonian H_3, while the numerical solutions employ Hamiltonian H_1. The following parameters are chosen: $\Omega = 2\pi \times 1\,\text{GHz}$ and $g = 2\pi \times 6\,\text{Hz}$. See Table 2 for detailed parameters.

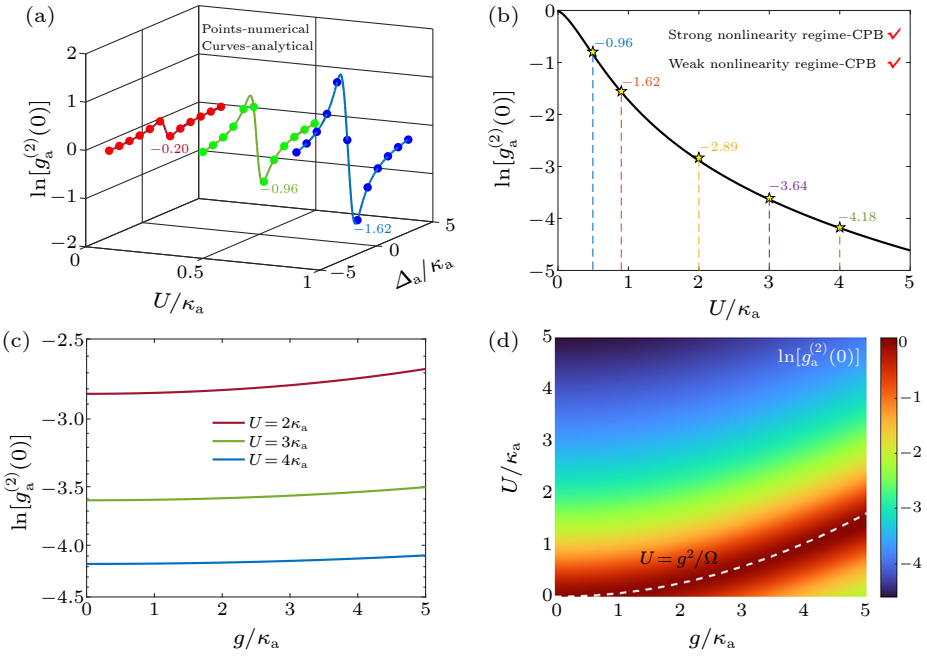

Fig. 3. (a) $\ln[g_{\rm a}^{(2)}(0)]$ versus $\Delta_{\rm a}/\kappa_{\rm a}$ for different values of U. Kerr nonlinear strength U is set to 0.1, 0.5, and 0.9 $\kappa_{\rm a}$. (b) $\ln[g_{\rm a}^{(2)}(0)]$ versus $U/\kappa_{\rm a}$. (c) $\ln[g_{\rm a}^{(2)}(0)]$ versus $g/\kappa_{\rm a}$ for different values of U. (d) $\ln[g_{\rm a}^{(2)}(0)]$ versus $g/\kappa_{\rm a}$ and $U/\kappa_{\rm a}$. Here, $\Omega = 2\pi \times 1\,\text{GHz}$, $\varepsilon = 0.01\kappa_{\rm a}$, and (b)–(d) $\Delta_{\rm a} = g^2/\Omega$. Other parameters are provided in Table 2.

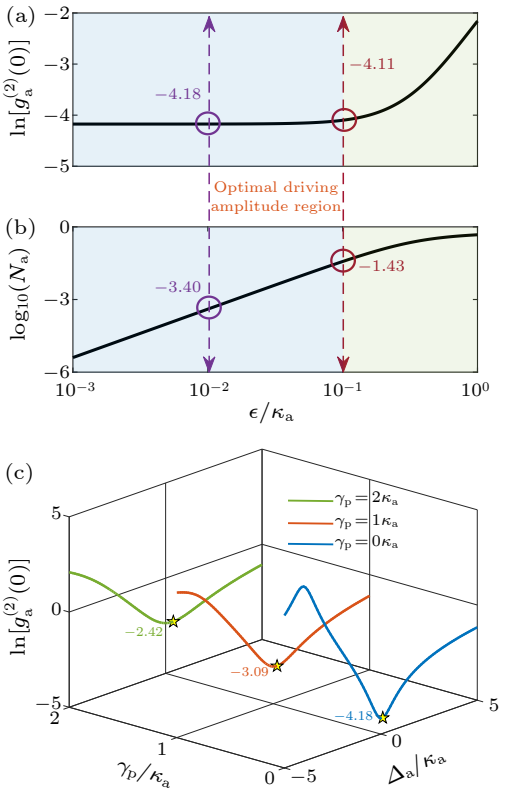

Fig. 4. (a) $\ln[g_a^{(2)}(0)]$ versus ε/κ_a. (b) $\log_{10}[N_a]$ versus ε/κ_a. (c) $\ln[g_a^{(2)}(0)]$ versus Δ_a/κ_a for different γ_p. Here, $U = 4\kappa_a$, (a) and (b) $\Delta_a = g^2/\Omega$. Other parameters are given in Table 2.

Table 2. Description of experimentally feasible parameters. For the related parameter detection, refer to Refs. [24,26–28].

Parameter	Value (all figures)
Driving amplitude ε/κ_a	0.01
Quality factor Q	3×10^6
Precession frequency $\Omega/2\pi$	1 (GHz)
Magnon mode decay rate $\gamma_m/2\pi$	1 (MHz)
Optical cavity mode frequency $\omega_a/2\pi$	193 (THz)
Optomagnonic coupling strength $g/2\pi$	6 (Hz)

Besides optomagnonic coupling strength g and Kerr nonlinear strength U, driving amplitude ε also plays a crucial role in the performance of a single-photon source. To achieve a high-quality single-photon source, it is necessary to maximize the intracavity average photon number while maintaining a good PB effect. This objective requires precise control of the driving amplitude to balance the PB effect and average photon number, thereby optimizing the performance of the single-photon source. As depicted in Fig. 4(a), both $g_a^{(2)}(0)$ and N_a increase with the enhancement of ε, gradually approaching Poissonian statistics. Consequently, to maximize the intracavity average photon number while achieving the PB effect, it is appropriate to select a weak driving condition. The results of the study indicated that the optimal region for the driving amplitude is located between $10^{-2}\kappa$ and $10^{-1}\kappa$. Up to this point in our analysis, we have not considered the effect of pure dephasing ($\gamma_p = 0$). Pure dephasing can originate from factors like a laser drive or thermal instability, causing perturbations in the polarization, linewidth, transmittance, and photon statistics. This effect can be effectively accounted for by incorporating an additional Lindblad term in the master equation, $\mathcal{L}[a^\dagger a]\rho = \gamma_p/2[2a^\dagger a\rho a^\dagger a - (a^\dagger a)^2\rho - \rho(a^\dagger a)^2]$, where γ_p is the pure dephasing rate for the optical cavity mode. Figure 4(b) depicts $g_a^{(2)}(0)$ as a function of the detuning Δ_a/κ_a for different values of the pure dephasing rate γ_p. It is observed that as pure dephasing rate γ_p increases, $g_a^{(2)}(0)$ gradually increases at the single-photon resonance transition (i.e., $\Delta_a = g^2/\Omega$). At a higher pure dephasing rate (e.g., $\gamma_p = 2\kappa$), our scheme can still generate the PB effect. This shows that our scheme can reliably prepare robust high-quality single-photon sources.

5. Conclusions. In conclusion, we investigated the CPB effect in a cavity optomagnonic system. Our study yielded the following three main conclusions. (i) With weak optomagnonic coupling, the CPB effect can be realized in both strong and weak Kerr nonlinear regimes. This finding relaxes the limitations on the experimental conditions and provides greater flexibility for experimental operations. (ii) In the parameter region where $U = g^2/\Omega$, the Kerr nonlinearity and Kerr-like nonlinearity of an optical cavity mutually cancel, making it impossible to achieve the PB effect within this parameter region. (iii) By precisely controlling the driving amplitude, it is possible to maximize the average intracavity photon number while maintaining a small photon equal-time second-order correlation function, thus generating high-quality single-photon sources with high purity and brightness. Our findings may provide an experimentally implementable method for observing the PB effect in a cavity optomagnonic system.

Acknowledgments. This work was supported by the Natural Science Foundation of Jilin Province (Grant No. 20240101013JC), the National Natural Science Foundation of China (Grant Nos. 62071412, 62475226, 62101479, 12074330, and 12375020), and the Young Talents Support Project of the Association of Science and Technology of Jilin Province (Grant No. QT202425).

References

[1] Wang Y P, Rao J W, Yang Y, Xu P C, Gui Y S, Yao B M, You J Q, and Hu C M 2019 *Phys. Rev. Lett.* **123** 127202
[2] Bai L, Harder M, Chen Y P, Fan X, Xiao J Q, and Hu C M 2015 *Phys. Rev. Lett.* **114** 227201
[3] Cao Y, Yan P, Huebl H, Goennenwein S T B, and Bauer G E W 2015 *Phys. Rev. B* **91** 094423
[4] Zhang W, Liu S T, Zhang S, and Wang H F 2024 *Phys. Rev. A* **109** 043712
[5] Hou R, Zhang W, Han X, Wang H F, and Zhang S 2024 *Phys. Rev. A* **109** 033721
[6] Ullah M and Mikki S 2024 *Phys. Rev. B* **109** 214303
[7] Xu J, Zhong C, Han X, Jin D, Jiang L, and Zhang X F 2021 *Phys. Rev. Lett.* **126** 207202
[8] Goryachev M, Farr W G, Creedon D L, Fan Y, Kostylev M, and Tobar M E 2014 *Phys. Rev. Appl.* **2** 054002
[9] Guan S Y, Wang H F, and Yi X 2022 *npj Quantum Inf.* **8** 102
[10] Li J, Zhu S Y, and Agarwal G S 2018 *Phys. Rev. Lett.* **121** 203601

[11] Zhang W, Wang T, Han X, Zhang S, and Wang H F 2022 *Opt. Express* **30** 10969
[12] Zhang W, Wang D Y, Bai C H, Wang T, Zhang S, and Wang H F 2021 *Opt. Express* **29** 11773
[13] Cheng J, Liu Y M, Yi X, and Wang H F 2022 *Ann. Phys.* **534** 2100493
[14] Li J, Zhu S Y, and Agarwal G S 2019 *Phys. Rev. A* **99** 021801
[15] Liu Z X, Xiong H, and Wu Y 2019 *Phys. Rev. B* **100** 134421
[16] Wang L, Yang Z X, Liu Y M, Bai C H, Wang D Y, Zhang S, and Wang H F 2020 *Ann. Phys.* **532** 2000028
[17] Zhang H X, Zhu S Y, Zhan J, Wang X J, Wang Y, Yao T, Mezin N I, and Song B 2023 *Chin. Phys. Lett.* **40** 127801
[18] Osada A, Hisatomi R, Noguchi A, Tabuchi Y, Yamazaki R, Usami K, Sadgrove M, Yalla R, Nomura M, and Nakamura Y 2016 *Phys. Rev. Lett.* **116** 223601
[19] Sharma S, Rameshti B Z, Blanter Y M, and Bauer G E W 2019 *Phys. Rev. B* **99** 214423
[20] Xu W L, Gao Y P, Cao C, Wang T J, and Wang C 2020 *Phys. Rev. A* **102** 043519
[21] Wu W J, Wang Y P, Wu J Z, Li J, and You J Q 2021 *Phys. Rev. A* **104** 023711
[22] Wang K, Gao Y P, Jiao R Z, and Wang C 2022 *Front Phys.* **17** 42201
[23] Hisatomi R, Osada A, Tabuchi Y, Ishikawa T, Noguchi A, Yamazaki R, Usami K, and Nakamura Y 2016 *Phys. Rev. B* **93** 174427
[24] Chai C Z, Shen Z, Zhang Y L, Zhao H Q, Guo G C, Zou C L, and Dong C H 2022 *Photonics Res.* **10** 820
[25] Liu T Y, Zhang X F, Tang H X, and Flatté M E 2016 *Phys. Rev. B* **94** 060405
[26] Viola-usminskiy S, Tang H X, and Marquardt F 2016 *Phys. Rev. A* **94** 033821
[27] Zhang X F, Zhu N, Zou C L, and Tang H X 2016 *Phys. Rev. Lett.* **117** 123605
[28] Osada A, Gloppe A, Hisatomi R, Noguchi A, Yamazaki R, Nomura M, Nakamura Y, and Usami K 2018 *Phys. Rev. Lett.* **120** 133602
[29] Yuan Z H, Chen Y J, Han J X, Wu J L, Li W Q, Xia Y, Jiang Y Y, and Song J 2023 *Phys. Rev. B* **108** 134409
[30] Xu W L, Liu X F, Sun Y, Gao Y P, Wang T J, and Wang C 2020 *Phys. Rev. E* **101** 012205
[31] Liu Z X, You C, Wang B, Xiong H, and Wu Y 2019 *Opt. Lett.* **44** 507
[32] Gao Y P, Cao C, Duan Y W, Liu X F, Pang T T, Wang T J, and Wang C 2020 *Nanophotonics* **9** 1953
[33] Hennrich M, Kuhn A, and Rempe G 2005 *Phys. Rev. Lett.* **94** 053604
[34] Hamsen C, Tolazzi K N, Wilk T, and Rempe G 2017 *Phys. Rev. Lett.* **118** 133604
[35] Zhang W, Wang T, Liu S T, Zhang S, and Wang H F 2023 *Sci. China Phys. Mech. Astron.* **66** 240313
[36] Winger M, Volz T, Tarel G, Portolan S, Badolato A, Hennessy K J, Hu E L, Beveratos A, Finley J, Savona V, and Imamoğlu A 2009 *Phys. Rev. Lett.* **103** 207403
[37] Shen S T, Li J H, and Wu Y 2020 *Phys. Rev. A* **101** 023805
[38] Liao J Q and Nori F 2013 *Phys. Rev. A* **88** 023853
[39] Wang D Y, Bai C H, Han X, Liu S T, Zhang S, and Wang H F 2020 *Opt. Lett.* **45** 2604
[40] Wang D Y, Bai C H, Xing Y, Liu S T, Zhang S, and Wang H F 2020 *Phys. Rev. A* **102** 043705
[41] Xie H, He L W, Shang X, Lin G W, and Lin X M 2022 *Phys. Rev. A* **106** 053707